ORIGINAL ARTICLE

JBMR®

Suppression of Autophagy by FIP200 Deletion Leads to Osteopenia in Mice Through the Inhibition of Osteoblast Terminal Differentiation

Fei Liu,[1] Fang Fang,[1] Hebao Yuan,[1] Dongye Yang,[1] Yongqiang Chen,[2] Linford Williams,[1] Steven A Goldstein,[3] Paul H Krebsbach,[1] and Jun-Lin Guan[2]

[1]Department of Biologic and Materials Sciences, University of Michigan School of Dentistry, Ann Arbor, MI, USA
[2]Division of Molecular Medicine and Genetics, Department of Internal Medicine, University of Michigan Medical School, Ann Arbor, MI, USA
[3]Orthopaedic Research Laboratories, Department of Orthopaedic Surgery, University of Michigan Medical School, Ann Arbor, MI, USA

ABSTRACT

Autophagy is a conserved lysosomal degradation process that has important roles in both normal human physiology and disease. However, the function of autophagy in bone homeostasis is not well understood. Here, we report that autophagy is activated during osteoblast differentiation. Ablation of focal adhesion kinase family interacting protein of 200 kD (FIP200), an essential component of mammalian autophagy, led to multiple autophagic defects in osteoblasts including aberrantly increased p62 expression, deficient LC3-II conversion, defective autophagy flux, absence of GFP-LC3 puncta in FIP200-null osteoblasts expressing transgenic GFP-LC3, and absence of autophagosome-like structures by electron microscope examination. Osteoblast-specific deletion of FIP200 led to osteopenia in mice. Histomorphometric analysis revealed that the osteopenia was the result of cell-autonomous effects of FIP200 deletion on osteoblasts. FIP200 deletion led to defective osteoblast terminal differentiation in both primary bone marrow and calvarial osteoblasts in vitro. Interestingly, both proliferation and differentiation were not adversely affected by FIP200 deletion in early cultures. However, FIP200 deletion led to defective osteoblast nodule formation after initial proliferation and differentiation. Furthermore, treatment with autophagy inhibitors recapitulated the effects of FIP200 deletion on osteoblast differentiation. Taken together, these data identify FIP200 as an important regulator of bone development and reveal a novel role of autophagy in osteoblast function through its positive role in supporting osteoblast nodule formation and differentiation. © 2013 American Society for Bone and Mineral Research.

KEY WORDS: OSTEOBLAST; AUTOPHAGY; DIFFERENTIATION; MOUSE; BONE DEVELOPMENT

Introduction

Autophagy is the primary intracellular degradation system. During autophagy, cytoplasmic materials are enclosed in a double-membraned structure, autophagosome, which will fuse with lysosome to form autolysosome, where degradation of the cytoplasmic materials occurs. Autophagy can be induced by starvation and other stresses to serve as a dynamic recycling system that produces new building blocks and energy for cellular renovation and homeostasis.[1] Besides its roles in adaptive responses to starvation, quality control of intracellular proteins and organelles, anti-aging, suppression of tumor formation, elimination of intracellular microbes, and antigen presentation, there is increasing evidence showing that autophagy also plays important roles in differentiation and development.[2,3] In mammals, autophagy is important for preimplantation development,[4] survival during neonatal starvation,[5] and cell differentiation during erythropoiesis,[6–8] lymphopoeisis,[9–12] and adipogenesis.[13–15]

The physiological and pathological roles of autophagy have been described for many organs.[1,16] However, the role of autophagy in bone is not well understood.[1,17] Osteoclasts, osteoblasts, and osteocytes are the three major bone cell types that are responsible for the maintenance of bone homeostasis.

Received in original form October 2, 2012; revised form March 21, 2013; accepted April 15, 2013. Accepted manuscript online April 30, 2013.
Address correspondence to: Fei Liu, DDS, PhD, Department of Biologic and Materials Sciences, University of Michigan School of Dentistry, 1011 N University Avenue, Ann Arbor, MI 48109, USA. E-mail: feiliu@umich.edu
Additional Supporting Information may be found in the online version of this article.

Journal of Bone and Mineral Research, Vol. 28, No. 11, November 2013, pp 2414–2430
DOI: 10.1002/jbmr.1971

There is emerging evidence implicating autophagy as an important mediator of bone cell function in normal physiology and pathology.[17–21] Recent studies suggest that autophagic mechanisms are active in osteocytes.[19,22–24] However, there is limited data to explain the physiological roles of autophagy in osteocyte homeostasis and skeletal maintenance.[17] A recent study elegantly demonstrated that some essential autophagy proteins, including Atg5, Atg7, Atg4B, and LC3, are important for generating the osteoclast ruffled border and bone resorption without affecting osteoclast differentiation.[25] This finding clearly links the autophagy genes with skeletal homeostasis. However, it is unclear whether the autophagy role of these proteins contributes directly to the aforementioned functions. The role of autophagy and/or autophagy proteins in osteoblast function is the least studied among the three major bone cell types. The closest clue came from the study of Nbr1, a selective autophagic receptor for degradation of ubiquitinated substrates. It has been shown that truncation of Nbr1 in a murine model, where it can interact with p62 but not LC3, leads to increased osteoblast differentiation and activity in vivo.[26] This study suggests the participation of autophagy in osteoblast function. Of note, Nbr1 is truncated globally but not osteoblast-specifically in this mouse model, which makes it unclear about the particular dependence of osteoblasts on autophagy. Thus, the direct roles of autophagy in osteoblast function are still unknown. In particular, it is currently unknown to what extent autophagy regulates osteoblast differentiation and bone development.

Focal adhesion kinase family interacting protein of 200 kD (FIP200) was initially identified as a protein inhibitor of focal adhesion kinase and its related kinase Pyk2.[27,28] Subsequent studies demonstrated that FIP200 also plays a role in the regulation of diverse cellular functions including cell size, survival, proliferation, spreading, and migration through its interaction with multiple cellular proteins.[29] Recently, several groups identified FIP200 as a component of the ULKs-Atg13-FIP200 complex, which is essential for the induction of autophagy in mammalian cells.[30–33] We showed that the defective phenotypes in mice with FIP200 conditional knockout in neurons[34] and hematopoietic stem cells[35] overlapped with those observed in mutant mice with deletion of other autophagy genes (eg, *Atg5* and *Atg7*) in these tissues.[8,36–39] Moreover, our recent studies demonstrated that suppression of autophagy by FIP200 deletion inhibits mammary tumorigenesis,[40] impairs DNA damage repair,[41] and depletes the postnatal neural stem cell pool.[42]

In this study, the observation that osteoblasts had high autophagy activity during nodule formation and differentiation in vitro led us to investigate the in vivo function of osteoblast autophagy. Because FIP200 global knockout leads to early embryonic lethality in mice,[43] we generated osteoblast-specific FIP200 conditional knockout mice to study the role of autophagy in bone development. Our data demonstrate that suppression of autophagy in osteoblasts by FIP200 deletion leads to compromised bone mass acquisition and osteoblast terminal differentiation. These results provide clear evidence for a positive role of autophagy in bone development and osteoblast differentiation.

Materials and Methods

Mice and skeleton preparation

The floxed FIP200 ($FIP200^{F/F}$), Osx-Cre, Col3.6-Cre, Col2.3-Cre, and GFP-LC3 transgenic mice were described previously.[43–46] All mice were backcrossed for at least eight generations onto a C57BL/6 background. $FIP200^{F/F}$ mice were mated with Osx-Cre, Col3.6-Cre, and Col2.3-Cre mice to generate $FIP200^{F/F}$;Osx-Cre, $FIP200^{F/F}$;Col3.6-Cre, and $FIP200^{F/F}$;Col2.3-Cre mice, designated as Osx-CKO, Col3.6-CKO, and Col2.3-CKO, respectively. Osx-CKO mice were further mated with GFP-LC3 mice to generate $FIP200^{F/F}$;Osx-Cre;GFP-LC3 mice, designated as Osx-CKO;GFP-LC3 mice. $FIP200^{F/F}$ mice and $FIP200^{F/F}$;GFP-LC3 mice served as control mice for Osx-CKO mice and Osx-CKO;GFP-LC3 mice, respectively. C57BL/6 mice (Charles River, Wilmington, MA, USA) served as wild-type control for Osx-Cre mice. Mice were housed under pathogen-free conditions, fed with 5001 or 5008 (for mating units) rodent diet (LabDiet, St. Louis, MO, USA) and handled according to local, state, and federal regulation. All experimental procedures were carried out with the approval of the Institutional Animal Care and Use Committee at the University of Michigan. Mice were euthanized by carbon dioxide overdose at 1 month, 2 months, 6 months, and 1 year old for bone phenotyping studies and at 6 to 8 weeks old for bone marrow cultures. Neonatal mice were euthanized by decapitation in primary calvarial osteoblast digestion experiments. The body weight of $FIP200^{F/F}$ and Osx-CKO mice were measured at birth, 1 week, 2 weeks, 1 month, 2 months, 3 months, 4 months, 5 months, 6 months, and 1 year (only for male) of age. Mice genotyping for FIP200 and Cre alleles were performed by polymerase chain reaction analysis of tail DNA as described previously.[35] Skeleton preparation with neonatal mice was performed as described previously.[47] In brief, after removal of the skin, viscera, and liver, the mice were fixed in 95% ethanol overnight and then stained in 0.15% Alcian Blue solution overnight, followed by 2 to 5 hours 95% ethanol treatment. Subsequently, the samples will be treated with 2% KOH for 24 hours or longer and then stained in 1% KOH, 0.015% Alizarin Red overnight. Skeletons will be cleared in 1% KOH, 20% glycerol for 2 days or more, and stored in a 1:1 mixture of glycerol and 95% ethanol.

Micro-computed tomography (micro-CT) analysis

Femurs and third lumbar (L3) vertebrae (endochondral bone) were dissected free of soft tissue and analyzed by micro-CT using an eXplore Locus SP (GE Healthcare Pre-Clinical Imaging, London, ON, Canada) as described previously.[48–50] In brief, femurs were scanned using the Parker method of rotation at 80 kVp and 80 μA and added filtration in the form of both an acrylic beam flattener and a 0.02-inch aluminum filter. Images were reconstructed at an isotropic voxel size of 18 μm (femora) and 16 μm (vertebrae) and calibrated daily (before scanning) using a phantom for densitometry. The metaphyseal/trabecular region of interest (ROI) from the distal femora is identified starting at the interface between the growth plate and metaphyseal trabecular bone and extending 10% of the bone length into the metaphysis using a splining algorithm in the transverse plane (MicroView v2.2, GE Healthcare Pre-Clinical Imaging). Trabecular

region of interest from the LC3 vertebrae is manually segregated from cortical bone by splining an areal region of interest at multiple levels and then interpolating among these to generate a volume of interest for the trabecular bone. Trabecular bone volume fraction (BV/TV), thickness (TbTh), number (TbN), and spacing (TbSp) were calculated after applying a constant threshold. For cortical analysis, a diaphyseal region of interest is identified using 18% of the bone length located in the center of the diaphysis of the femur and corresponding precisely to the location of the midpoint of the four-point bending loads that will be applied for mechanical testing. Cortical thickness and endosteal and periosteal perimeters were then calculated after applying a uniform threshold. Beam hardening (particularly in the cortical regions) is minimized by the combination of the beam flattener and aluminum filter.[51]

Calvaria thickness measurement

Calvaria (intramembranous bone) thickness was measured at the center of parietal bone with Pfingst Original Iwanson Gauge (Lincoln Dental, Cherry Hill, NJ, USA) directly on 1 month, 2 months, and 6 months old mice in a blind manner. Six measurements were taken on each calvaria with three on each side of parietal bone.

Femoral biomechanical testing

The four-point bending test was performed as described previously.[52,53] Femora were loaded in the anterior–posterior direction so that the posterior side of the bone was in tension and the anterior side was in compression. In brief, each bone was tested on a specially adapted MTS Servo-Hydraulic Testing Machine (MTS Systems, Eden Prairie, MN, USA) that includes a substructure to test mouse bones. Tests were conducted at a constant rate of displacement equal to 0.5 mm/second. Load from a high-resolution load cell and displacement from a linear variable differential transformer were directly acquired in a microcomputer. Utilizing algorithms developed in MatLab, the load-deformation data were analyzed for a variety of mechanical property measures. All bones were tested while moist and at room temperature. The following calculations were made: 1) load to failure (yield load and ultimate load); 2) bending stiffness, determined from a linear regression performed on the "pre-yield" portion of the load-displacement curve (the term "yield" is used here to refer to the point in the test when the load-displacement curve departs from a relatively linear course by 10%); 3) energy to failure.

Histomorphometry

Static and dynamic histomorphometry were performed as described previously.[54,55] For dynamic histomorphometry, mice were given intraperitoneal injections of calcein (10 mg/kg) and xylenol orange (90 mg/kg) 6 days and 2 days, respectively, before euthanization, and the measurement was made at femur cortical bone. All static and dynamic parameters were measured according to the Report of the American Society of Bone and Mineral Research Histomorphometry Nomenclature Committee.[56]

Primary calvarial osteoblast isolation and culture

Calvarial cells were isolated from 1- to 3-day-old transgenic mice. After removal of sutures, parietal bones of calvariae were subjected to four sequential digestions. The first two digestions were in an enzyme mixture containing 1 mg/mL collagenase A (Roche, Indianapolis, IN, USA) and 2 mg/mL Dispase II (Roche) at 37°C on a rocking platform. The last two digestions were in an enzyme mixture containing 2 mg/mL collagenase A and 2 mg/mL Dispase II. Cell fractions (3 to 4) were collected and enzyme activity was stopped by addition of an equal volume of α modified essential medium (a-MEM; Gibco by Life Technologies, Grand Island, NY, USA) containing 10% heat-inactivated fetal bovine serum (FBS; HyClone, Thermo Scientific, Waltham, MA, USA; SH30070.03), 100 U/mL of penicillin, and 100 mg/mL of streptomycin (Gibco BRL, Grand Island, NY, USA). The fractions were centrifuged, resuspended in a-MEM containing 10% heat-inactivated FBS, and filtered through a 70-μm cell strainer. Cells were plated in a density of 1.9 to 2.4×10^4 cells/cm^2 in 6-cm dish in a-MEM containing 10% heat-inactivated FBS. Twenty-four hours later, the medium was changed. Three days later, the cells were trypsinized and plated at a density of 1.5×10^4 cells/cm^2 in 35-mm culture plates in a-MEM containing 10% FBS. For autophagy flux experiments, the lysosomal inhibitor NH_4Cl (30 mM) or Chloroquine (100 μM) were added to cells for indicated length. For differentiation experiments, the medium was changed 3 days later and thereafter every 2 days. At 1 week of culture, the medium was changed to differentiation medium (a-MEM containing 10% FBS, 50 mg/mL of ascorbic acid, and 4 mM of beta-glycerophosphate). In some of the differentiation experiments, autophagy inhibitor 3-MA (2 mM) or Chloroquine (5 μM) was added to the culture from day 4 to day 21. The autophagy inhibitor concentration was selected by their effectiveness in inhibiting the basal autophagy in primary calvarial osteoblasts.

LC3 conversion and turnover assay[57]

Primary calvarial osteoblasts were cultured in a-MEM containing 10% heat-inactivated FBS. To determine the steady-state levels of LC3II expression, the cells were treated with or without lysosomal inhibitor, NH_4Cl (30 mM), for the indicated time. Cell lysates were subjected to immunoblot analysis with an anti-LC3 antibody. For turnover assay, the starved cells were treated with or without Chloroquine (100 μM) for 3 hours. The difference in LC3-II levels between samples with and without Chloroquine was compared.

Bone marrow culture

Femurs and tibias from 6- to 8-week-old mice were dissected from surrounding tissues. The epiphyseal growth plates were removed and marrow collected by flushing with serum-free a-MEM containing 100 U/mL penicillin and 100 μg/mL streptomycin with a 25-gauge needle. Cells were plated in a density of 1×10^6 cells/cm^2 in 35-mm culture plates in a-MEM containing 10% heat-inactivated FBS. Half of the medium was changed on day 3. On day 7, the medium was changed to differentiation medium (a-MEM containing 10% FBS, 50 mg/mL of ascorbic acid, and 8 mM of beta-glycerophosphate) and thereafter the medium

was changed every 2 days until day 21. In some of the differentiation experiments, autophagy inhibitor 3-MA (2 mM) or Chloroquine (15 μM) was added to the culture from day 3 to day 7 or from day 10 to day 21 as indicated. The autophagy inhibitor concentration was selected by their effectiveness in inhibiting the basal autophagy in mouse bone marrow osteoblasts. In another set of differentiation experiments, FAK inhibitor, PF-573,228,[58] or FAK, Pyk2 dual inhibitor, PF-562,271[59] (generously provided by Pfizer, Inc., New York, NY, USA), was added to the culture from day 7 to day 21 at the pharmacologically effective concentration of both 1 μM and 5 μM.

Histochemical analysis of cell cultures

Histochemical staining for ALP activity was performed using a commercially available kit (86-R Alkaline Phosphatase; Sigma Diagnostics, Inc., St. Louis, MO, USA) according to the manufacturer's instructions. Mineralization was assessed using modified Alizarin red (AR-S) staining method. Briefly, cells were fixed for 1 hour with ice-cold 70% ethanol and washed with water. Then the cells were stained with 40 mM AR-S, pH 4.2, at room temperature for 10 minutes with rotation. The unbound AR-S were washed with water. To quantify the staining, 10% w/v cetylpyridinium chloride (CPC) was added to elute the bound AR-S for 30 minutes at room temperature. Aliquots of these AR-S extracts were then diluted (in 10% CPC) and the concentration determined by absorbance measurement at 562 nm on a plate reader.

Starvation

For starvation, cells were washed with amino acid-free Earle's balanced salt solution (EBSS; HyClone, SH30029.02) without FBS (starvation medium) and incubated with the same medium. The cells were starved 15 to 60 minutes for steady state autophagy activity assay, 3 hours for autophagy flux assay and GFP-LC3 puncta assay, and 6 hours for transmission electron microscopy examination.

Transmission electron microscopy

Samples were prepared as described previously with minor modification.[34] In brief, cells were fixed in 2.5% glutaraldehyde in 0.1 M Sorensen's buffer, pH 7.4, overnight at 4°C. They were then postfixed in 1% osmium tetroxide and rinsed in double distilled water and then stained with aqueous 1% uranyl acetate for 1 hour. The samples were dehydrated in ethanol, rinsed two times in propylene oxide, and embedded in epoxy resin. They were ultrathin-sectioned at 70 nm in thickness and stained with uranyl acetate and lead citrate. The sections were examined and recorded as described previously.[34,40] In brief, 37 to 46 sections per group were randomly chosen to measure the mitochondria size, number, and cytoplasmic area. Mitochondria number was normalized by cytoplasmic area. Mitochondria size was the average of 312 to 476 individual mitochondria.

Western blot analysis

Protein extracts were prepared from calvaria, heart, liver, growth plate at distal femur, and proximal tibia of neonatal mice, femur (after bone marrow flushing), heart, liver of 1-month-old mice, primary calvarial osteoblasts isolated from neonatal mice (between at birth and postnatal day 3), and mouse embryonic fibroblast (MEF) cells. Cells and tissues were lysed using NP40 lysis buffer (pH 8.0 Tris-HCl 20 mM, NaCl 137 mM, 1% NP40, 10% glycerol, Na_3VO_4 1 mM), and protein extracts were analyzed by 8% (FIP200, vinculin), 10% (P62), and 18% (LC3) SDS-PAGE and blotted onto PVDF membrane (Millipore, Billerica, MA, USA, IPVH00010). Membranes were incubated with rabbit anti-RBCC1 (FIP200) antibody (Proteintech, Chicago, IL, USA, 17250-1-AP), rabbit anti-P62 antibody (Enzolife Science, Farmingdale, NY, USA, BML-PW9860-0100), mouse anti-LC3 antibody (Nanotools, Germany, NT-0231-100), or mouse anti-vinculin antibody (Sigma-Aldrich, V4505) followed by horseradish peroxidase-conjugated secondary antibody (goat anti-rabbit, Thermo Scientific, 31460, and goat anti-mouse, Jackson ImmunoResearch [West Grove, PA, USA], 115-035-072) and developed with HPR substrate ECL (Millipore, WBKL S0500).

Immunofluorescence and fluorescence microscopy

Immunofluorescent staining was performed as described previously.[41] Anti-Ki67 antibody was purchased from Spring Bioscience (Pleasanton, CA, USA, M3062). Primary calvarial osteoblasts isolated from GFP-LC3 transgenic mice were observed directly with a fluorescence microscope (Olympus BX51, Japan). The fluorescent images were taken with Olympus DP70 camera. The same exposure time was used in the same experiment when pictures were taken.

RNA extraction and qRT-PCR

Total RNA was isolated using Trizol reagent (Invitrogen) according to the manufacturer's instructions. For qRT-PCR analyses, equal amounts of RNA were reverse-transcribed by SuperScript III first-strand synthesis system (Invitrogen) with oligo(dT) as a primer, and then the resulting cDNA templates were subjected to qRT-PCR using the SYBR Green PCR Core reagents system (Qiagen, Valencia, CA, USA) with the following primers: ALP (alkaline phosphatase), BSP (bone sialoprotein), OCN (osteocalcin), Osx (osterix), and 18SRNA. Primer sequences are listed in Supplemental Methods.

Statistical analysis

Mann-Whitney test was used to compare two test groups, and differences were considered significant for $p < 0.05$.

Results

Autophagy is activated during osteoblast nodule formation and differentiation

As a first step to test whether autophagy plays a role in osteoblast differentiation, we assessed the dynamic autophagy activation during osteoblast differentiation. First, we determined the autophagy flux by measuring the conversion of the cytosolic form of LC3 (LC3-I) to the autophagosome-bound form of LC3 (LC3-II) in the absence and presence of a lysosomal inhibitor, NH_4Cl, with lysate collected at different differentiation stages (Fig. 1*A* and Supplemental Fig. S1). LC3-II was detected in the

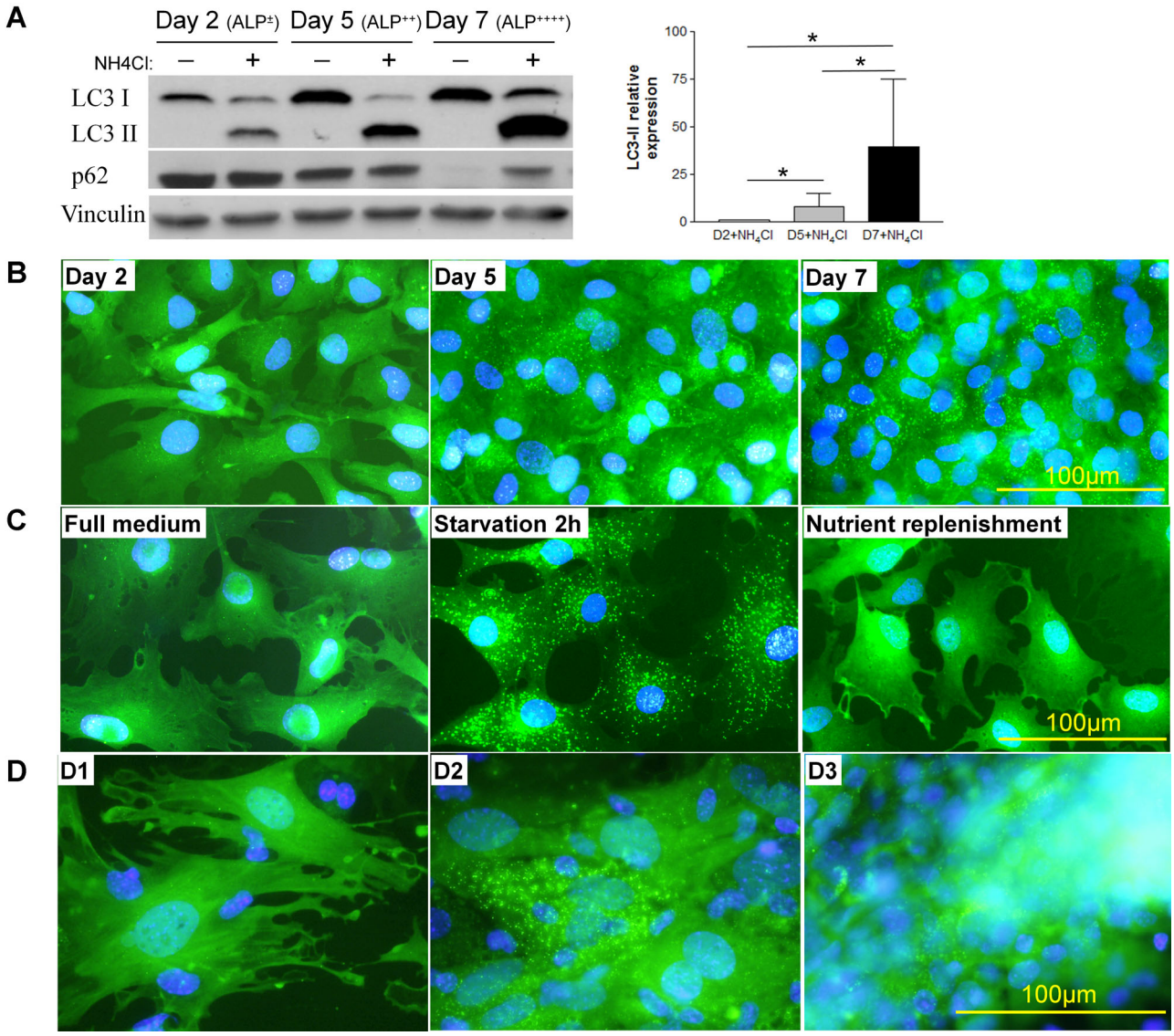

Fig. 1. Autophagy is activated during osteoblast differentiation. (*A*) Lysates isolated from primary calvarial osteoblasts at indicated different differentiation stages with or without 2-hour 30-mM NH_4Cl treatment were analyzed by Western blotting using anti-LC3 (top), anti-p62 (middle) or anti-vinculin (bottom) antibodies. Graph on the right shows the quantification of LC3-II expression (normalized to vinculin expression). $^*p < 0.05$, $n = 3$. (*B*) Primary calvarial osteoblasts were isolated from GFP-LC3 transgenic mice, fixed, and analyzed under fluorescent microscope at indicated day after plating. (*C*) Primary calvarial osteoblasts isolated from neonatal GFP-LC3 transgenic mice were cultured in complete or starvation medium for 2 hours or starvation medium for 2 hours followed by 2-hour complete medium at day 2 cultures before having reached confluence. The cells were then fixed, stained with Dapi, and subject to fluorescent microscope analysis. (*D*) Bone marrow cells were isolated from 6- to 8-week-old GFP-LC3 transgenic mice and subject to osteogenic differentiation until day 11. D1 shows the isolated osteoblast like cells in the culture. D2 shows the slightly condensed osteoblast-like cell nodule. D3 shows the highly condensed osteoblast-like cell nodule. The data shown were the representatives of at least three independent experiments.

presence but not in the absence of NH_4Cl and its level increased with time (Fig. 1*A*), suggesting that autophagy flux increases in the differentiation process. In agreement with an increase in autophagy flux, we observed decreased expression of p62, a selective autophagy substrate at a later differentiation time point. Second, we examined GFP-LC3 puncta, representing autophagosome formation, during differentiation with primary calvarial osteoblasts isolated from neonatal GFP-LC3 mice.[46] There were few cells that had positive GFP puncta before cells reached confluence, suggesting a low steady-state autophagy. However, GFP puncta dramatically increased after osteoblasts reached confluence (Fig. 1*B*), suggesting a much higher steady-state autophagy in osteoblasts during the cell cluster/nodule formation process. Of note, we performed GFP puncta and LC3-II conversion experiments at the indicated time points 2 hours after fresh medium changes to avoid the potential confounding factor of nutrient deprivation in long-term cultures. As a control, we replenished nutrient medium for 2 hours in previously starved subconfluent cultures and observed the complete disappearance of GFP-LC3 puncta (Fig. 1*C*). Third, we examined the GFP-LC3 punta formation in bone marrow stromal cell culture from GFP-LC3 mice.[46] In the same culture, we observed very little GFP-LC3 puncta in the cells that had not formed cluster/colony (Fig. 1*D*1). However, there were numerous GFP-

LC3 puncta in the cells that were undergoing cluster/nodule formation (Fig. 1*D*2) and mineralization (Fig. 1*D*3). Altogether, these data demonstrated that there is higher level of steady-state autophagy and autophagic flux during osteoblast nodule formation and differentiation, suggesting an important role of autophagy in this process.

Ablation of FIP200 in osteoblasts leads to autophagy deficiency

To assess the physiological significance of autophagy activation in osteoblasts, we generated conditional knockout mice to delete FIP200, an essential mammalian autophagy gene in osteoblasts. Briefly, we mated floxed FIP200 ($FIP200^{F/F}$) mice[43] with Osx-Cre transgenic mice[44] to generate $FIP200^{F/F}$;Osx-Cre mice (designated as Osx-CKO mice). Osx-Cre mice express Cre recombinase in osteoprogenitor cells committed to the osteoblast lineage.[44] Osx-CKO and littermate control ($FIP200^{F/F}$) mice were born with a normal Mendelian ratio (data not shown). As a first step to characterize this mouse model, we evaluated autophagy deficiency in FIP200-null osteoblasts with several complementary approaches. First, we examined the expression of p62, a selective autophagy substrate in primary calvarial osteoblasts isolated from Osx-CKO mice. We observed increased p62 expression in the osteoblasts isolated from Osx-CKO mice (designated as CKO cells or CKO osteoblasts) (Fig. 2*A*), suggesting an autophagy defect in these cells. Of note, FIP200 was nearly completely deleted in CKO osteoblasts, indicating that CKO cells are FIP200-null cells (Fig. 2*A*). Second, we examined the steady-state autophagy in CKO osteoblasts. In control cells, 30 and 60 minutes of amino acid and serum starvation induced LC3 conversion (Fig. 2*B*). In contrast, the starvation-induced LC3 conversion was abolished in CKO cells. Third, we determined autophagy flux by LC3 turnover assay. Consistent with the role of FIP200 in the initiation of autophagosome formation, LC3-II protein levels were significantly lower under starvation and in the presence of chloroquine in CKO cells compared with control cells (Fig. 2*C*), indicating a defective autophagy flux in CKO cells. Fourth, we isolated primary calvarial osteoblasts from Osx-CKO and control mice bearing transgenic GFP-LC3 and examined GFP-LC3 puncta formation after 2 hours of starvation. As expected, we observed robust GFP-LC3 puncta forming in osteoblasts isolated from control mice, but this was absent in osteoblast isolated from Osx-CKO;GFP-LC3 mice (Fig. 2*D*). Lastly, to further confirm the effects of loss of FIP200 on autophagosome formation, we performed transmission electron microscopic analysis. We detected autophagic vacuoles in about 30% of the control osteoblasts (Fig. 2*E*, upper and lower left). In contrast, autophagosome-like structures were absent in CKO cells (Fig. 2*E*, lower right).

To investigate the effects of starvation on osteoblast mitochondria, the cells were subjected to 6-hour starvation. In control cells, mitochondria size increased (Fig. 2*F*), area decreased (Fig. 2*G*), and number decreased (Fig. 2*H*) in response to 6-hour starvation, which is consistent with the notion that mitochondria elongate and are partly degraded through autophagy during starvation.[60] Interestingly, we found that the mitochondria were enlarged in CKO cells (Fig. 2*F*) without obvious difference in number (Fig. 2*H*). In CKO cells, the mitochondria size did not increase but decreased instead in response to starvation (Fig. 2*F*). Mitochondria area decrease (Fig. 2*G*) in these cells was proportional to the mitochondria size decrease, suggesting that the mitochondria area decrease in these cells was because of the mitochondria size decrease. In contrast to the significant decrease in mitochondria number in control cells, there was no change in CKO cells in response to 6-hour starvation, further supporting the autophagy deficiency in these cells. Taken together, these data suggested that FIP200-null osteoblasts were deficient in autophagy.

FIP200 deletion leads to osteopenia in mice

Osx-CKO and littermate control ($FIP200^{F/F}$) mice were born with similar body weight (Supplemental Fig. S2). However, by as early as 1 week, both male and female Osx-CKO mice weighed less than controls. This weight differential was extended over the 6 to 12 months of observation. To investigate the effects of FIP200 deficiency on bone development, we first evaluated deletion of FIP200 by Western blotting of lysates from tissues of Osx-CKO and control neonatal mice. As shown in Supplemental Fig. S3, a significantly reduced level of FIP200 was found in the calvaria but not heart and liver samples from Osx-CKO mice compared with control mice, indicating efficient and specific deletion of FIP200 as expected. We then performed whole mount skeleton staining of newborn mice. Compared with control bones, Osx-CKO mice had no obvious developmental defects in major skeletal elements including humerus, radius, and ulna (Supplemental Fig. S4*A*), femur, tibia, and fibula (Supplemental Fig. S4*B*), ribs and vertebrae (Supplemental Fig. S4*C*), suggesting that bone formation was not affected at this stage of development. Next, we used micro-CT to evaluate the effects of FIP200 deletion on postnatal bone morphometry. Micro-CT analysis revealed an osteopenic phenotype in Osx-CKO mice. In femur trabecular bone of Osx-CKO female mice, we observed a decrease (59%, 37%, and 53% at 1, 2, and 6 months, respectively) in trabecular bone volume (BV/TV) (Fig. 3*A*), a decrease (52%, 33%, and 52% at 1, 2, and 6 months, respectively) in trabecular number (TbN) (Fig. 3*B*), a slight decrease (14% and 9% at 1 and 2 months, respectively) in trabecular thickness (TbTh) (Fig. 3*C*), and an increase (172%, 57%, and 129% at 1, 2, and 6 months, respectively) in trabecular spacing (TbSp) (Fig. 3*D*). In femur cortical bone of Osx-CKO mice, we observed a decrease (17%, 23%, and 23% at 1, 2, and 6 months, respectively) in cortical thickness (Fig. 3*E*), a decrease (16%, 9%, and 11% at 1, 2, and 6 months, respectively) in outer cortical bone perimeter (Fig. 3*F*), and a decrease (16%, 6%, and 6% at 1, 2, and 6 months, respectively) in inner cortical bone perimeter (Fig. 3*G*). Besides the femurs, we performed micro-CT analysis on 1-month-old L3 vertebrae and observed similar phenotype. There was a 34%, 21%, and 17% decrease in trabecular bone volume, trabecular number, and trabecular thickness, respectively, in Osx-CKO mice (Supplemental Fig. S5). In addition to the endochondrally formed bones, we also examined calvaria (intramembranous bone). The calvarial thickness of CKO mice was significantly decreased compared with controls (Fig. 3*H*). Similar osteopenic phenotype was observed in male mutant mice (Supplemental Fig. S6). To

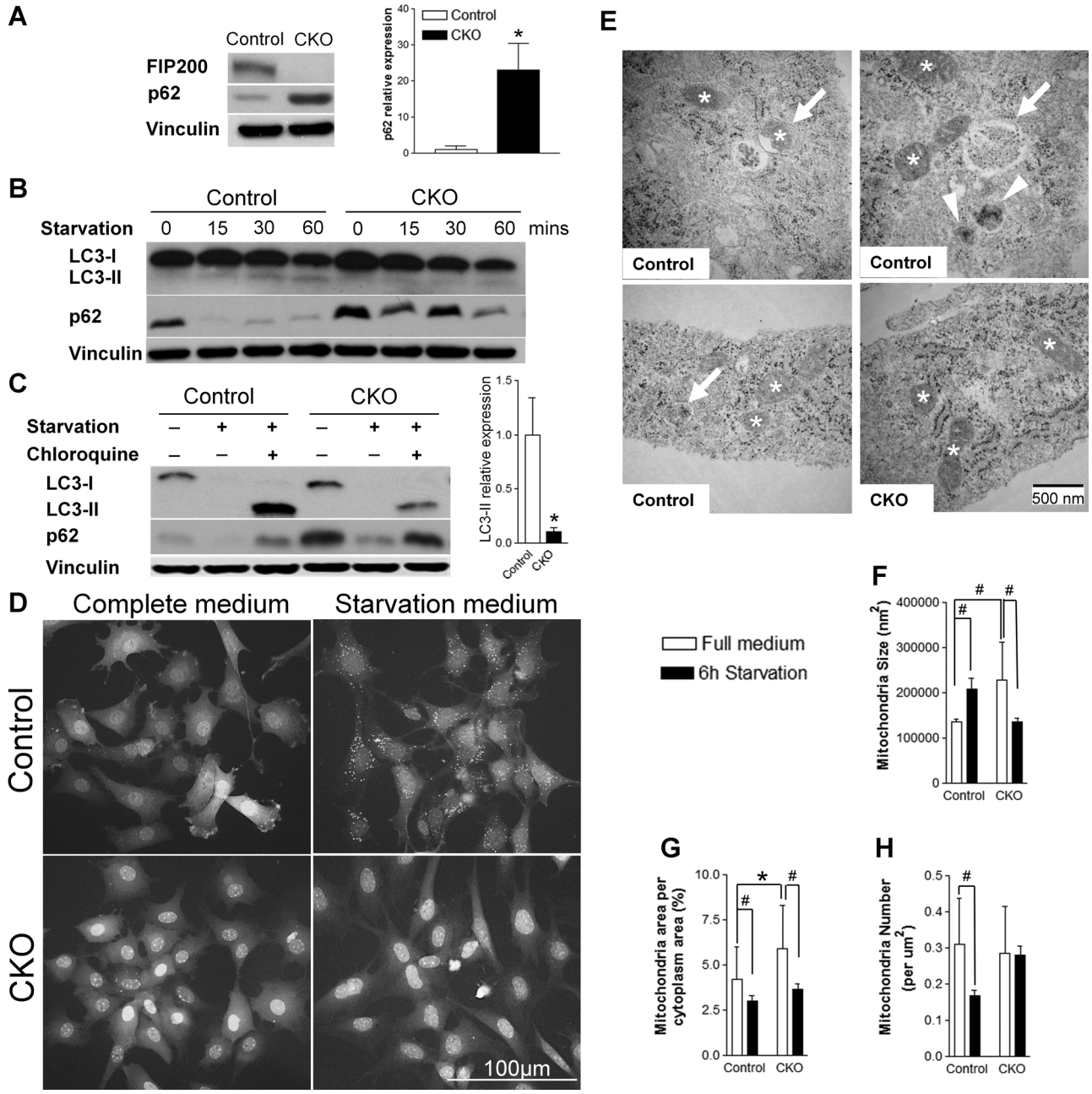

Fig. 2. FIP200-null osteoblasts are autophagy deficient. (*A*) Primary calvarial osteoblasts were isolated from control or Osx-CKO neonatal mice and cultured in complete medium for 3 days. Cell lysates were subjected to immunoblot analysis with indicated antibodies. Graph on the right shows the quantification of p62 expression (normalized to vinculin expression). (*B*) Primary calvarial osteoblasts were cultured in complete medium or starvation medium (serum and amino acid–free EBSS) for up to 60 minutes. Cell lysates were subjected to immunoblot analysis with indicated antibodies. (*C*) Control and FIP200-null primary calvarial osteoblasts were cultured in the complete or starvation medium for 3 hours with or without 100 μM chloroquine. The cell lysates were subjected to immunoblot analysis with indicated antibodies. Graph on the right shows the quantification of LC3-II expression with starvation and chloroquine treatment. (*D*) Control and FIP200-null primary calvarial osteoblasts isolated from mice expressing transgenic GFP-LC3 were cultured in complete medium or starvation medium for 120 minutes and then were observed directly with a fluorescence microscope after fixation. (*E*) Transmission electron microscopic image of control and FIP200-null primary calvarial osteoblasts. Arrows point to autophagosome-like structure, arrowheads point to autolysosome-like structure, and asterisks indicate mitochondria. (*F–H*) Primary calvarial osteoblasts were isolated from neonatal control or Osx-CKO mice. Osteoblasts were cultured in complete or starvation medium for 6 hours and then fixed and subjected to EM analysis and quantification. (*F*) Mitochondria size. $^{\#}p < 0.001$, $n = 312–476$ per group. (*G*) Mitochondria area per cytoplasmic area. $^{*}p < 0.01$, $^{\#}p < 0.001$, $n = 37–46$ per group. (*H*) Mitochondria number. $^{\#}p < 0.001$, $n = 37–46$ per group. For *F–H*, the data were presented as mean ± SD. Western blotting and immunofluorescence data shown were the representative of three independent experiments. All experiments were performed before cells had reached confluence.

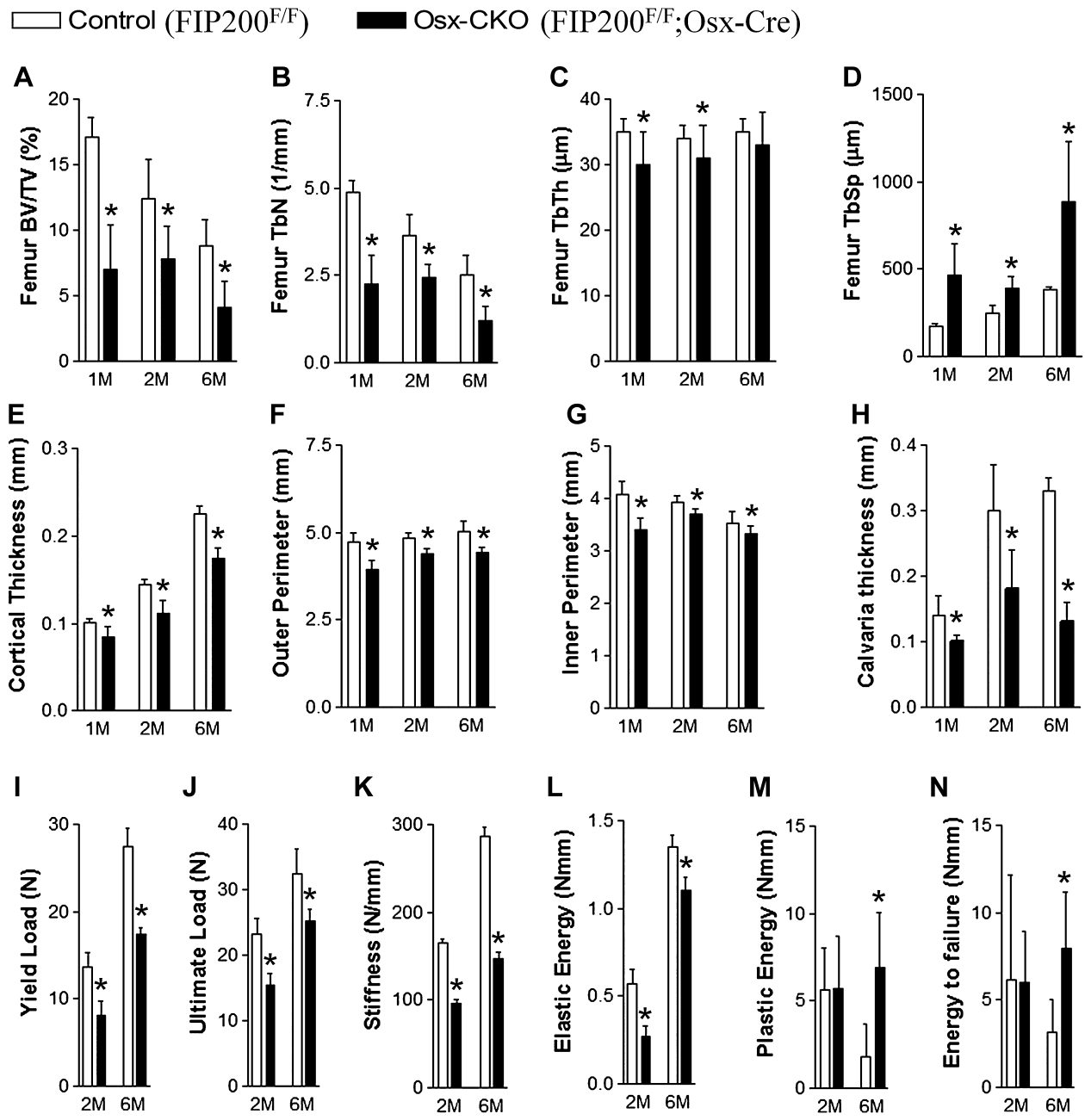

Fig. 3. FIP200 deletion in osteoblasts leads to severe osteopenia in mice. (*A–G*) Trabecular and cortical parameters were determined by micro-CT for the femurs from 1-month-old (1M) to 6-month-old (6M) Osx-CKO female mice: (*A*) bone volume/tissue volume (BV/TV); (*B*) trabebular number (TbN); (*C*) trabecular thickness (TbTh); (*D*) trabecular spacing (TbSp); (*E*) cortical bone thickness; (*F*) cortical bone outer perimeter; (*G*) cortical bone inner perimeter. (*H*) Calvarial bone thickness was directly measured with caliper. (*I–N*) Four-point bending test with femurs: (*I*) yield load; (*J*) ultimate load; (*K*) stiffness; (*L*) elastic energy; (*M*) plastic energy; and (*N*) energy to failure. For each group, $n = 6–9$, $^{*}p < 0.05$. Data are mean ± SD.

determine to what extent the low bone mass phenotype was owing to the Osx-Cre transgene itself, we analyzed the femur and vertebrae L3 of Osx-Cre mice and their littermate control mice. Except the slightly decreased outer and inner femur cortical perimeters, Osx-Cre mice had comparable cortical and trabecular bone parameters compared with the control mice (Supplemental Fig. S7), suggesting that the phenotype observed in Osx-CKO mice was largely because of the deletion of FIP200. To further confirm that the observed phenotype was indeed resulting from the specific deletion of FIP200 in osteoblasts, we used other lines of osteoblast-targeting Cre transgenic mice, including Col3.6-Cre and Col2.3-Cre[45] to delete FIP200 in osteoblasts and observed a similar osteopenic phenotype in FIP200$^{F/F}$;Col3.6-Cre (Col3.6-CKO) mice (data not shown) and FIP200$^{F/F}$;Col2.3-Cre (Col2.3-CKO) mice (Supplemental Fig. S8*A–D*), highlighting the role of FIP200 in osteoblast functions. As expected, significantly reduced level of FIP200 was found in femur but not heart and liver samples from Col2.3-CKO mice compared with control mice (Supplemental Fig. S8*E*). In addition, FIP200-null osteoblasts isolated from Col2.3-CKO mice demonstrated similar autophagy

deficiency (Supplemental Fig. S8*F, G*) as the cells isolated from Osx-CKO mice. Taken together, our data demonstrated that FIP200 deletion in osteoblasts leads to compromised bone development and decreased bone mass in mice.

To determine the extent to which FIP200 deletion would affect the mechanical properties of bone, we tested the femurs of Osx-CKO and control mice by four-point bending.[52] Femurs of female mutant mice had decreased yield load (Fig. 3*I*), decreased ultimate load (Fig. 3*J*), decreased stiffness (Fig. 3*K*), and decreased elastic energy (Fig. 3*L*). In contrast, increased plastic energy and total failure energy were noted in the 6-month-old mutant group (Fig. 3*M, N*), which may be an adaptive response or just a reflection of a change in the properties of the extracellular matrix. Similar mechanical property changes were also found in femurs of mutant male mice (Supplemental Fig. S3*I–L*). Interestingly, the bones of the 6-month-old mutant male mice had comparable yield load (Supplemental Fig. S3*I*) and ultimate load (Supplemental Fig. S3*J*), which is consistent with the comparable cortical bone thickness at this stage (Supplemental Fig. S3*E*). Collectively, these data demonstrated that bones in FIP200 mutant mice had significantly altered mechanical properties with decreased strength to resist fracture compared with that of control mice.

Decreased bone formation and compromised osteoblast terminal differentiation are responsible for the osteopenic phenotype in Osx-CKO mice

To determine the cellular mechanisms of FIP200 regulation on bone metabolism, we performed histomorphometry on femurs of Osx-CKO and control mice. Consistent with micro-CT measurements, we observed decreased bone area (BA/TA) (Fig. 4*A*), decreased trabecular number (TbN) (Fig. 4*B*), and increased trabecular spacing (data not shown) in the femur of Osx-CKO mice. The osteoblast number (Nob/BS) (Fig. 4*C*) and surface (ObS/BS) (Fig. 4*D*) but not the osteoclast number (NOc/BS) (Fig. 4*E*) and surface (OcS/BS) (Fig. 4*F*) were reduced by the deletion of FIP200 in Osx-CKO mice. Dynamic histomorphometry analysis revealed decreased bone formation in Osx-CKO mice (Fig. 4*G–J*). Collectively, these data suggest that compromised osteoblast bone formation in vivo contributed to decreased bone mass in Osx-CKO mice.

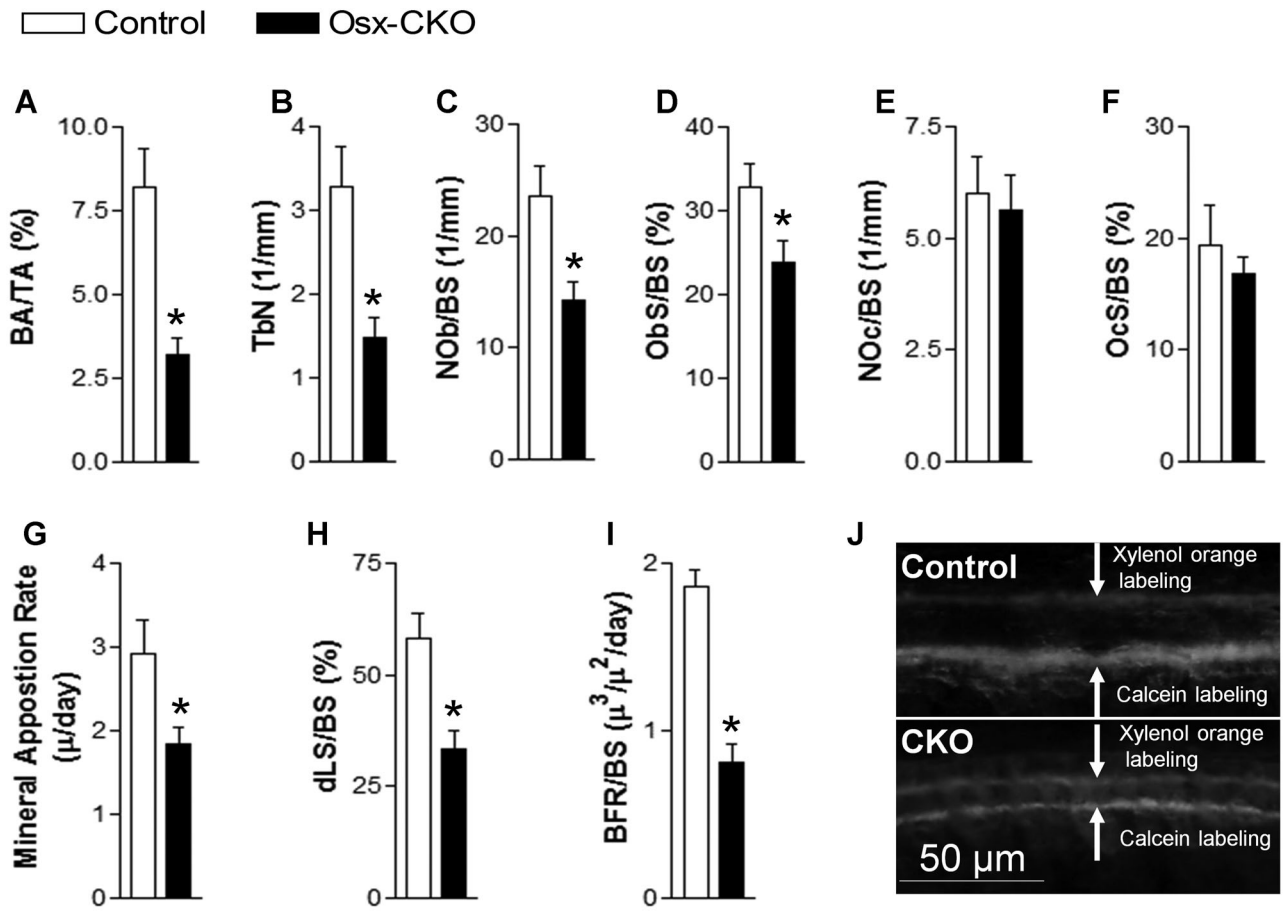

Fig. 4. FIP200 deletion in osteoblasts leads to decreased bone formation. (*A–F*) Static histomorphometry for the femurs of 1-month-old female Osx-CKO and control mice: (*A*) trabecular bone area/tissue area (BA/TA); (*B*) trabecular bone number (TbN); (*C*) osteoblast number per bone surface (NOb/BS); (*D*) osteoblast surface per bone surface (ObS/BS); (*E*) osteoclast number per bone surface (NOc/BS); (*F*) osteoclast surface per bone surface (OcS/BS). (*G–J*) Dynamic histomorphometry for the femurs of 1-month-old female Osx-CKO and control mice: (*G*) mineral apposition rate; (*H*) double labeling surface per bone surface (dLS/BS); (*I*) decreased bone formation rate (BFR/BS); (*J*) representative calcein and xylenol orange double labeling image (5 days apart between two labelings). $^{*}p < 0.05$, $n = 5–7$ per group.

To further determine the mechanism responsible for the decreased bone formation observed in Osx-CKO mice, we investigated the effect of FIP200 deletion on osteoblast differentiation with two in vitro primary osteoblast culture systems. First, we found that bone marrow stromal cells isolated from Osx-CKO mice had compromised terminal differentiation as shown by Alizarin Red staining (Fig. 5*A, B*). The expression levels of osteoblast differentiation markers, including alkaline phosphates (ALP), bone sialoprotein protein (BSP), and osteocalcin (OCN), as well as the osteoblast transcription factor Osterix (Osx) were significantly decreased in the CKO cultures (Fig. 5*C*). In another complementary approach, we isolated bone marrow stromal cells from $FIP200^{F/F}$ mice and infected them with an adenovirus encoding Cre (Ade-Cre) or Laz (Ade-Laz) after 7 days' culture (preosteoblastic colonies have been formed at this stage). In the FIP200-null group (Ade-Cre), we observed compromised mineralization (Fig. 5*D, E*), as well as decreased expression of osteoblast differentiation markers (Fig. 5*F*), suggesting that FIP200 plays a critical role at a later stage of differentiation. To further confirm the role of FIP200 in later osteoblast differentiation stages, we isolated primary calvarial osteoblasts from neonatal mice and cultured them in osteogenic medium. Interestingly, we found that the early differentiation of FIP200-null calvarial osteoblasts was not compromised, as indicated by the comparable alkaline phosphatase staining pattern (Fig. 5*G*) and alkaline phosphatase (ALP, early osteoblast differentiation marker) mRNA expression level (Fig. 5*H*). However, terminal osteoblast differentiation was greatly compromised (Fig. 5*I–K*). In addition, we observed similar differentiation defect in the primary calvarial osteoblasts isolated from Col2.3-CKO neonatal mice (Supplemental Fig. S8*H*). Together, these data demonstrated that FIP200 deletion led to compromised osteoblast terminal differentiation.

To determine whether the compromised differentiation was the result of defective proliferation in FIP200-null osteoblasts, we used the primary calvarial osteoblast culture system to evaluate the effects of FIP200 deletion on proliferation by Ki67 staining. We found comparable Ki67-positive cells in FIP200-null and control osteoblasts (Fig. 6*A, B*), indicating that FIP200 deficiency did not affect primary calvarial osteoblast proliferation. Consistent with the similarities in proliferation, there was a similar increase in cell number in both groups during early culture periods (Fig. 6*C*). However, CKO cell number increased much slower after the cells reached confluence (day 3 to day 4) and there were significantly fewer cells in CKO group at the end of 21 days of culture, suggesting the decreased osteoblast number may be partly responsible for compromised mineralization. However, after normalizing the calcium concentration shown in Fig. 5*J* with cell numbers shown in Fig. 6*C*, there is still a 65% decrease in mineralization in the CKO group, suggesting CKO cells had compromised mineralization ability. Furthermore, at late culture stages (day 21), as a result of condensational growth and concomitant terminal differentiation, the control cells formed large mineralized nodules. In contrast, FIP200-null cells formed fewer and much smaller nodules (Fig. 6*D*), suggesting a defect in the nodule formation process. To determine the extent to which FIP200 deletion affected the osteoblast nodule formation ability, we evaluated the osteoblastic colony growth in bone marrow culture with alkaline phosphatase staining. We found that the size of alkaline phosphatase-positive osteoblastic colonies in the CKO group was similar to control cells at early culture (day 7 and day 10) but was smaller at later stages of culture (day 14) (Fig. 6*E, G*). Unexpectedly, we found there were more alkaline phosphatase-positive colonies in CKO cultures (Fig. 6*E, F*), which may be owing to the effects of FIP200 deletion on early osteoblast progenitor cells. The total alkaline phosphatase-positive area was correspondingly larger in early CKO cultures but not in late (day 14) cultures because of the significantly decreased colony size (Fig. 6*H*). The increased alkaline phosphatase-positive osteoblasts in early culture and compromised ability to grow in later culture associated with compromised mineralization suggest an inability of osteoblasts to switch from proliferation to mineralization upon FIP200 deletion. The compromised ability to grow after having reached confluence in primary calvarial osteoblasts and defective colony growth in bone marrow osteoblasts suggest that FIP200-null osteoblasts had a compromised ability to undergo the maturation process. Taken together, the above data indicated that FIP200 deletion adversely affected osteoblast nodule formation, leading to defective terminal differentiation and compromised bone formation ability.

Autophagy inhibitors mimic the effect of FIP200 deletion on osteoblast differentiation

The aforementioned data demonstrated that autophagy is activated during osteoblast differentiation (Fig. 1) and FIP200-null osteoblasts had nodule formation deficiency (Fig. 6). Considering the positive role of autophagy in contributing to the adaptive response of cells under stress, these data support the notion that suppression of autophagy by FIP200 deletion is responsible for the compromised osteoblast differentiation. To test this hypothesis, we used two autophagy inhibitors, including 3-methyladenine (3-MA) and chloroquine, to determine whether autophagy indeed plays an important role in osteoblast differentiation.

Because we found that FIP200 deficiency had no effect on osteoblastic colony size at day 10 bone marrow culture but led to decreased colony size at day 14 (Fig. 6*E, G*), we started to treat bone marrow cells with 2 mM 3-MA or 15 μM chloroquine at day 10 and examined its effect on early differentiation by alkaline phosphatase staining at day 14 and mineralization by Alizarin Red staining at day 21 (Fig. 7*A*). We found that both 3-MA and chloroquine treatment caused a decrease in the number of alkaline phosphatase-positive cells and led to smaller colony size (Fig. 7*A*) compared with the control cultures, similar to the bone marrow cells isolated from Osx-CKO mice (Fig. 6*E*). Consistent with the decrease in alkaline phosphatase staining–positive cells, there was a significant decrease in mineralization at day 21 (Fig. 7*A*), a mirror image of the bone marrow cells isolated from Osx-CKO mice (Fig. 5*A, D*). To determine whether the autophagy inhibitors had any cytotoxic effect on bone marrow cells, bone marrow cells were treated with 2 mM 3-MA or 15 μM chloroquine at day 7 culture and then counted at day 9. No adverse effects of inhibitor treatment on bone marrow cell number were observed (Fig. 7*B*), suggesting the defective osteoblast differentiation in 3-

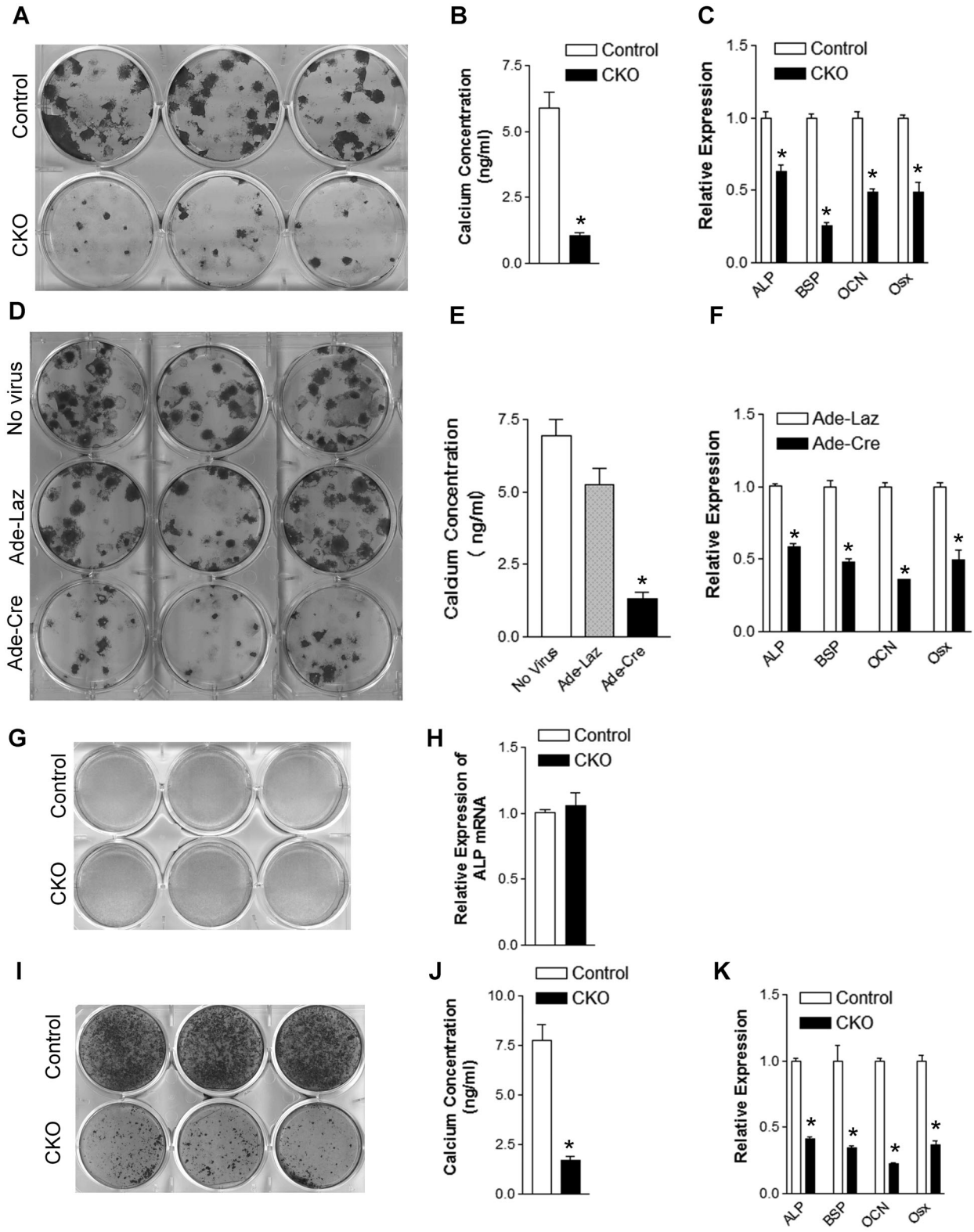

Fig. 5. FIP200 deletion compromises osteoblast terminal differentiation. (*A–C*) Bone marrow cells were collected from 6- to 8-week-old control or Osx-CKO mice and subject to osteoblast differentiation: (*A*) Representative Alizarin Red staining image at the end of 21 days of osteogenic culture. (*B*) Quantified calcium concentration for the samples in (*A*). (*C*) Osteoblast differentiation marker expression in cultures shown in (*A*). (*D–F*) Bone marrow cells from FIP200$^{F/F}$ mice were infected with adenovirus encoding Cre (Ade-Cre) or Laz (Ade-Laz) after 7 days of osteogenic culture: (*D*) Representative Alizarin Red staining image at the end of 21 days of culture. (*E*) Quantified calcium concentration for the samples in (*D*). (*F*) Osteoblast differentiation marker expression in the cultures shown in (*D*). (*G–K*) Primary calvarial osteoblast cultures: (*G*) Early osteoblast differentiation was evaluated by Alkaline phosphatase staining at day 7 culture. (*H*) Early osteoblast differentiation marker (Alkaline phosphatase mRNA) was determined by quantitative PCR. (*I*) Representative Alizarin Red staining image at the end of 21 days of osteogenic culture. (*J*) Quantified calcium concentration for the samples in (*I*). (*K*) Osteoblast differentiation marker expression in cultures shown in (*I*). Data are the representatives of three independent experiments with triplicates for each experiment. $^{*}p < 0.05$, $n = 3$ per group.

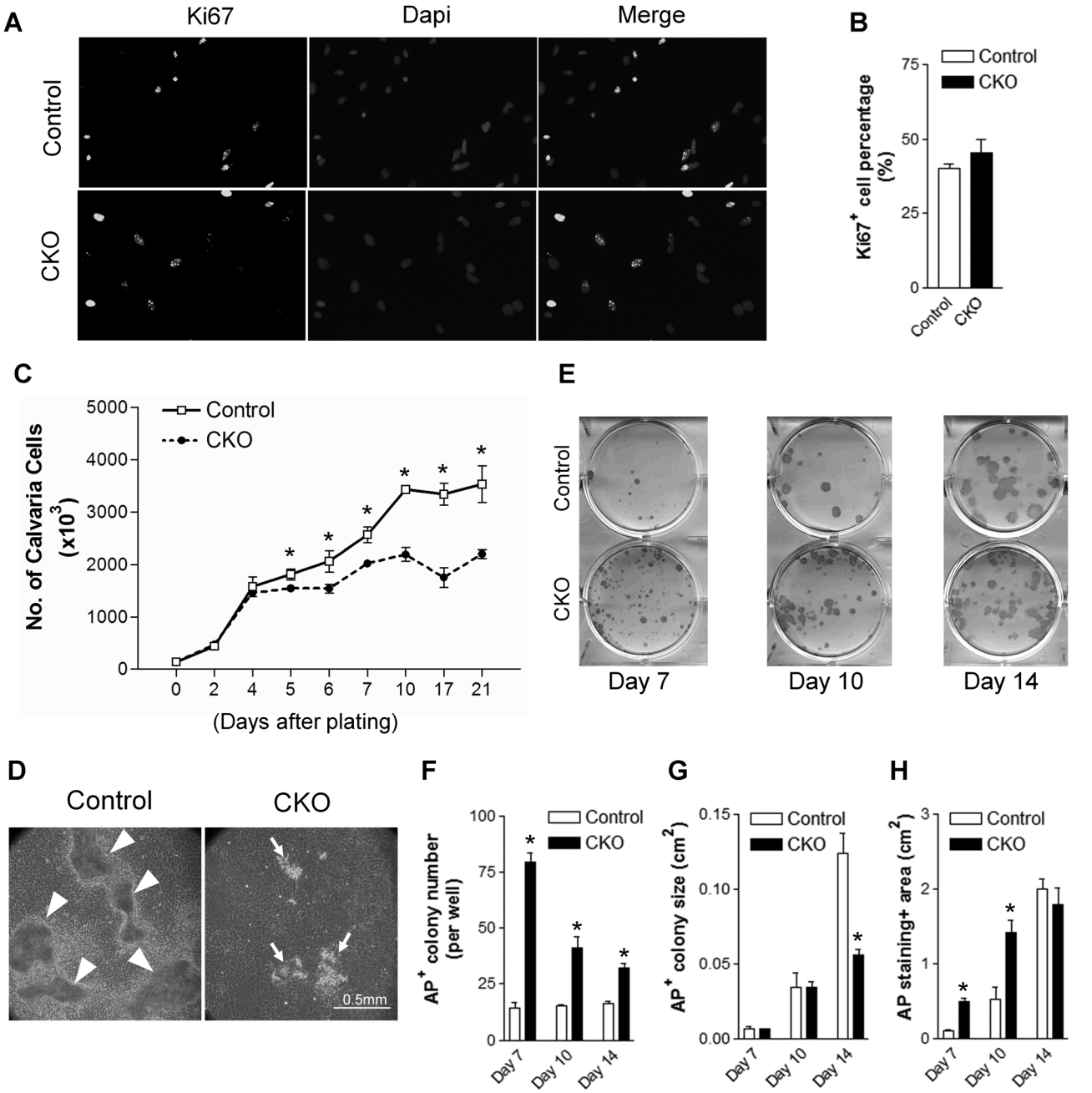

Fig. 6. FIP200 deficiency compromises the osteoblast nodule formation. (*A, B*) Immunostaining with anti-Ki67 antibody was performed in the primary osteoblasts isolated from neonatal calvaria of Osx-CKO and control mice. (*A*) Representative fluorescent images. (*B*) Quantitative data of the Ki67-positive osteoblasts. (*C, D*) Primary calvarial osteoblasts were isolated from neonatal control or Osx-CKO mice and cultured in osteogenic medium for 3 weeks: (*C*) Cell numbers were counted at indicated time point. (*D*) Representative images showing the nodule formation at the end of 21 days of culture. Arrowheads indicate the big nodules in control culture, and arrows indicate the small nodules in Osx-CKO culture. (*E–H*) Bone marrow cells were collected from 6- to 8-week-old control or Osx-CKO mice and subject to osteoblast differentiation: (*E*) Alkaline phosphatase staining at indicated time points. (*F*) Quantitative Alkaline phosphatase-positive (ALP^+) osteoblastic colony numbers at indicated time points as shown in (*E*). (*G*) Quantitative AP^+ osteoblastic colony size at indicated time points as shown in (*E*). (*H*) Quantitative ALP^+ area at indicated time points as shown in (*E*).

MA- or chloroquine-treated bone marrow culture was not because of a cytotoxic effect. In addition, we treated the bone marrow cells with 2 mM 3-MA from day 3 until day 7 (Fig. 7*C*) and performed alkaline phosphatase staining at day 7. We found that the 3-MA treatment had no effect on the alkaline phosphatase-positive colony number and size (Fig. 7*C*). This indicated that 3-MA treatment had no effect on the early bone marrow osteoblast differentiation when the colony was small and not dense. The comparable colony size at early culture and compromised late differentiation in 3-MA-treated bone marrow osteoblasts suggest the autophagy plays an important role in late osteoblast differentiation. In addition to examining the effects of autophagy inhibition on bone marrow osteoblast differentiation, we determined the effects of autophagy inhibition on primary

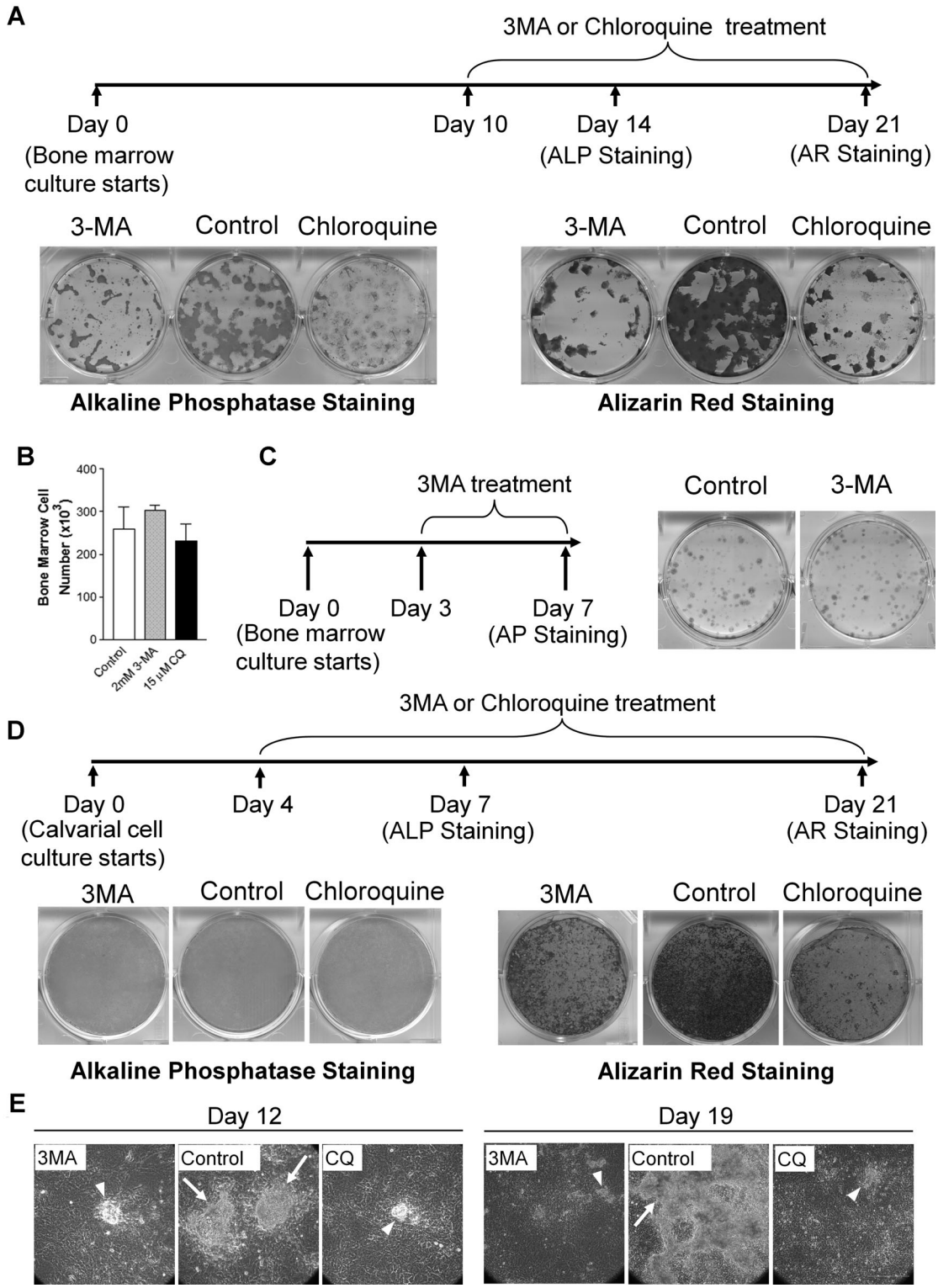

Fig. 7. Inhibition of autophagy leads to compromised osteoblast differentiation. (*A–C*) Bone marrow cells were isolated from 6- to 8-week-old C57/BL6 mice and subject to osteogenic culture. (*A*) Diagram of the inhibitor treatment (2 mM 3MA or 15 μM chloroquine) scheme (late treatment) and the representative images of Alkaline phosphatase staining and Alizarin Red staining results. (*B*) Bone marrow cells were treated with autophagy inhibitors at indicated dose starting from day 7 for 2 days, and cell numbers were counted at day 9. (*C*) Diagram of the inhibitor treatment scheme (early treatment) and the representative Alkaline phosphatase staining result. (*D*) Primary calvarial osteoblasts were isolated from neonatal C57/BL6 mice and subject to osteogenic culture. Diagram shows the inhibitor treatment (2 mM 3MA or 5 μM chloroquine) scheme, and images show the representative Alkaline phosphatase staining and Alizarin Red staining results. (*E*) Primary calvarial osteoblasts were isolated from neonatal control or Osx-Cre mice and cultured in osteogenic medium. For the control cells, one group was treated with 2 mM 3MA and the other group was treated with 5 μM chloroquine. Phase contrast images were taken at indicated time points (D12 and D19 culture). Arrows point to the big nodule in control culture. Arrowheads point to the small nodule in autophagy inhibitor-treated culture. Scale bar = 0.25 mm.

calvarial osteoblast differentiation (Fig. 7*D*). Two mM 3-MA or 5 μM chloroquine treatment had no obvious adverse effect on early osteoblast differentiation (Fig. 7*D*, lower left) but compromised the terminal differentiation at day 21 culture (Fig. 7*D*, lower right), similar to the observation in primary calvarial osteoblasts isolated from Osx-CKO mice (Fig. 5*G, I*). Additionally, we found that the autophagy inhibitor treatment did not affect the cell number increase at early culture (data not shown), indicating that the defective osteoblast terminal differentiation was not because of the cytotoxic effect. Lastly, we determined the effects of autophagy inhibition on the nodule-formation ability of primary calvarial osteoblasts. Both 2-mM 3-MA and 5-μM chloroquine treatment negatively affected condensed nodule formation, mimicking the effect of FIP200 deletion (Fig. 7*E*). Altogether, autophagy inhibition with both 3-MA and chloroquine recapitulated the effect of suppression of autophagy by FIP200 deletion on osteoblast differentiation, strongly supporting the notion that FIP200 regulates osteoblast differentiation through its autophagy function.

Discussion

Autophagy, the major intracellular degradation system, has been implicated in many physiological and pathological processes. It has gained attention recently as an essential contributor to human health and disease.[1,16,61,62] Compared with our understanding of the role of autophagy in many organs, little is known about how autophagy regulates bone physiology and disease. The global knockout of many autophagy genes in mice, including Ambra1,[63] Atg5,[5] Atg7,[64] Beclin,[65] and FIP200,[43] leads to early lethality, preventing us from studying the physiological role of autophagy in bone development. In this study, we overcame this limitation by generating FIP200 conditional KO mice with three different Cre transgenic mouse lines targeting osteoblast lineage cells, including Osx-Cre,[44] Col3.6-Cre, and Col2.3-Cre.[45] A similar osteopenia phenotype was observed in all transgenic lines, highlighting the important role of FIP200 in bone development and osteoblast function. Our data provide a rigorous and direct demonstration of the positive role of autophagy in osteoblast differentiation.

As expected, we observed that FIP200-null osteoblasts were autophagy deficient. However, in contrast to the reported deformed mitochondria in Atg7-deficient hepatic cells[64] and FIP200-deficient mammary tumor cells,[40] we did not notice obvious mitochondria deformation in CKO cells, whereas we found that the mitochondria size was increased in these cells. This suggested a cell type–specific effect of autophagy deficiency on mitochondria morphology. In response to 6-hour starvation, mitochondria size increased significantly but the mitochondria area decreased significantly in control cells, which is consistent with the recent finding that mitochondria elongate during starvation.[60] Through fusion, mitochondria have bigger size in an elongated form during starvation. In the meantime, the mitochondria with smaller size are easier to be eliminated through autophagy. We also found that mitochondria number in control cells decreased greatly (46%) in response to 6-hour starvation, which is likely owing to both the elongation and autophagic degradation of mitochondria. In CKO cells, the mitochondria size did not increase but decreased instead. This size decrease may be mediated through the autophagy function of FIP200 or alternatively through the potential direct role of FIP200 in mitochondria itself. The mitochondria number in CKO cells was not changed in response to 6-hour starvation, suggesting that mitochondria were not degraded in these cells through autophagy. However, it is important to note that mitochondria could be degraded in CKO cells through other autophagy-independent mechanisms such as proteasomal degradation machinery or as a consequence of induction of the apoptotic pathway.[66]

The essential role of FIP200 in autophagy in many mammalian cell types is well documented.[30–33,67] Our data demonstrated the requirement of FIP200 in osteoblast autophagy. We also showed that treatment with autophagy inhibitors recapitulated the effects of FIP200 deletion on osteoblast nodule formation and terminal differentiation. These data strongly suggest that FIP200 regulates osteoblast function through its autophagy role. However, it is still possible that FIP200 may regulate osteoblast differentiation at least partially through its nonautophagic roles. FIP200 was originally identified by our group as an inhibitor of FAK and its related kinase Pyk2.[27,28] Because both FAK and Pyk2 have been shown to regulate osteoblast function,[68,69] this raised the possibility that FIP200 regulates osteoblast differentiation through FAK/Pyk2. However, it was shown that FAK does not play an important role in osteoblast differentiation, although it regulates bone healing.[68] On the other hand, it was shown that Pyk2 can regulate osteoblast differentiation but it only has the inhibitory effect on early osteoblast progenitor cells but not on more mature primary calvarial osteoblast.[69] Our data clearly showed that the effect of FIP200 deletion on osteoblast differentiation was at later stage but not early stage. Therefore, it is not likely that FIP200 regulates osteoblasts mainly through Pyk2. We still cannot exclude the possibility that the increased FAK and/or Pyk2 activity in FIP200-null osteoblast may account at least partly for the observed differentiation defect because previous studies only examined the effect of FAK knockdown (but not overexpression) on osteoblast differentiation. However, we found that FAK inhibitor[58] and FAK, Pyk2 dual inhibitor[59] failed to rescue the defective differentiation in FIP200 Osx-CKO bone marrow culture, although the higher concentration of both inhibitors negatively affected the osteoblast differentiation (Supplemental Fig. S9), suggesting the osteoblast differentiation defect in FIP200-null cells was not because of increased FAK and/or Pyk2 activity.

During development and differentiation, enhanced autophagic degradation is often required to cope with the drastic cellular and tissue remodeling.[1] Here, we report that autophagy is activated during osteoblast nodule formation and differentiation and suppression of autophagy by FIP200 deletion leads to severely compromised bone formation with defective osteoblast differentiation. Furthermore, the suppression of autophagy by FIP200 deletion led to decreased osteoblastic colony size and decreased osteoblast nodule size in bone marrow and primary calvaria cultures, respectively. These data suggested an inability of osteoblasts to switch from initial proliferation to mineralization upon FIP200 deletion. During terminal differentiation process, osteoblasts secrete abundant extracellular matrix with

active protein synthesis. mTOR signaling is the major pathway to regulate protein synthesis. Protein synthesis and autophagic degradation are usually regulated in an opposite manner by mTOR. Activated mTOR facilitates the protein synthesis and inhibits autophagy.[70,71] However, it is recently reported that protein degradation and synthesis may be spatially coupled in certain cells that have increased protein secretion, such as podocytes and differentiating macrophagy. It is delicately shown that autophagy-generated amino acids contribute to the mTOR recruitment and activity.[72] Thus, the catabolic (autophagy) machinery could augment the anabolic (mTOR) machinery and facilitate the mass synthesis of secretory proteins. This raised the interesting possibility that osteoblasts may utilize autophagy in the same manner to facilitate the robust protein synthesis, which is crucial for their terminal differentiation. Furthermore, we demonstrated that the autophagy inhibition by known autophagy inhibitors mimicked the effects of FIP200 deletion on osteoblast differentiation and nodule/colony formation ability in vitro, supporting the hypothesis that FIP200 regulates osteoblast differentiation through its autophagy role. Interestingly, the suppression of autophagy either by FIP200 deletion or administration of autophagy inhibitors did not affect early osteoblast differentiation when the osteoblastic colony size is relatively small and cells are not dense. This suggests the development/differentiation stage–dependent role of autophagy in osteoblast differentiation.

In CKO mice, we found that there was 57% BV/TV decrease in younger (1 month) male mice, whereas there was only 39% decrease in older (1 year) mice. The smaller difference at older age may be explained by the decreased autophagy efficiency in the wild-type osteoblasts of older mice, similar to the phenomenon observed in other cell types.[73] However, the autophagy efficiency of osteoblasts from aged animal needs to be determined to address this possibility. The alternative possibility is that the bigger effect of FIP200 deletion on early bone development may be owing to the higher requirement of autophagy in active bone growth phase.

Our data demonstrated that autophagy deficiency in osteoblasts led to compromised osteoblast differentiation and mineralization, and it may suggest that autophagy dysregulation may be one causal factor for bone disease such as osteoporosis. In line with the findings in our mouse models, a recent pathway-based genome-wide association study identified the association between regulation-of-autophagy pathway with human wrist bone mineral density and osteoporosis.[20] It is generally assumed that the autophagy level decreases as a result of aging.[73] It is tempting to propose to increase autophagy to treat aging-associated osteoporosis. In fact, a recent attempt to increase autophagy by inhibiting mTOR signaling pathway leads to improved cognitive function in a mouse model of Alzheimer disease.[74] Recently, a candidate therapeutic peptide that can induce autophagy in vivo in peripheral tissues in adult mice was identified.[75] Strikingly, this peptide can improve the clinical outcome of mice with virus infection by enhancing autophagy. This raises the interesting possibility that similar approaches could be applied to bone disorders.

In conclusion, our studies identified an important role of FIP200, an essential autophagy gene, in bone development in several mouse models. We demonstrated that the ablation of FIP200 in osteoblasts inhibited osteoblast differentiation through negatively affecting osteoblast nodule formation and mineralization ability. These results provide novel insight into the regulation of bone development and osteoblast differentiation by autophagy. However, there are still many unanswered questions that need to be addressed: What are the detailed molecular mechanisms by which autophagy regulates osteoblast functions? What are the roles of autophagy in late postnatal bone development? What are the roles of autophagy in bone disease such as osteoporosis? How does aging affect the osteoblast autophagy activity? Answers to these questions will greatly help in better understanding the pathogenesis of bone diseases and may reveal novel ways to treat age-induced bone loss.

Disclosures

All authors state that they have no conflicts of interest.

Acknowledgments

We thank Drs Sean Morrison for providing Osx-Cre transgenic mice, Chenran Wang and Li Wang for comments on the manuscript, Ms Basma Khoury and Dr Zhou Wang for micro-CT measurement, and Ms Jaclynn Kreider for micro-CT measurement and mechanical test.

FL was supported by the National Institute of Arthritis and Musculoskeletal and Skin Diseases of the National Institutes of Health under award number R01AR062030 and Rackham Faculty Research Grant (Rackham Graduate School, University of Michigan). PHK was supported by the National Institutes of Health under award number R01DK082481. JG was supported by the National Institutes of Health under award numbers GM052890 and CA150926.

Authors' roles: Study design: FL. Study conduct: FL, FF, HY, DY, and YC. Data collection: FL, FF, HY, and DY. Data analysis: FL, FF, PHK, SAG, and LW. Data interpretation: FL, PHK, SAG, and JG. Drafting manuscript: FL. Approving final version of manuscript: FL, FF, HY, DY, YC, LW, SAG, PHK, and JG. FL takes responsibility for the integrity of the data analysis.

References

1. Mizushima N, Komatsu M. Autophagy: renovation of cells and tissues. Cell. 2011;147(4):728–41.
2. Cecconi F, Levine B. The role of autophagy in mammalian development: cell makeover rather than cell death. Dev Cell. 2008;15(3):344–57.
3. Mizushima N, Levine B. Autophagy in mammalian development and differentiation. Nat Cell Biol. 2010;12(9):823–30.
4. Tsukamoto S, Kuma A, Murakami M, Kishi C, Yamamoto A, Mizushima N. Autophagy is essential for preimplantation development of mouse embryos. Science. 2008;321(5885):117–20.
5. Kuma A, Hatano M, Matsui M, Yamamoto A, Nakaya H, Yoshimori T, Ohsumi Y, Tokuhisa T, Mizushima N. The role of autophagy during the early neonatal starvation period. Nature. 2004;432(7020):1032–6.
6. Sandoval H, Thiagarajan P, Dasgupta SK, Schumacher A, Prchal JT, Chen M, Wang J. Essential role for Nix in autophagic maturation of erythroid cells. Nature. 2008;454(7201):232–5.

7. Zhang J, Randall MS, Loyd MR, Dorsey FC, Kundu M, Cleveland JL, Ney PA. Mitochondrial clearance is regulated by Atg7-dependent and -independent mechanisms during reticulocyte maturation. Blood. 2009;114(1):157–64.
8. Mortensen M, Ferguson DJ, Edelmann M, Kessler B, Morten KJ, Komatsu M, Simon AK. Loss of autophagy in erythroid cells leads to defective removal of mitochondria and severe anemia in vivo. Proc Natl Acad Sci USA. 2010;107(2):832–7.
9. Pua HH, Guo J, Komatsu M, He YW. Autophagy is essential for mitochondrial clearance in mature T lymphocytes. J Immunol. 2009;182(7):4046–55.
10. Stephenson LM, Miller BC, Ng A, Eisenberg J, Zhao Z, Cadwell K, Graham DB, Mizushima NN, Xavier R, Virgin HW, Swat W. Identification of Atg5-dependent transcriptional changes and increases in mitochondrial mass in Atg5-deficient T lymphocytes. Autophagy. 2009;5(5):625–35.
11. Pua HH, Dzhagalov I, Chuck M, Mizushima N, He YW. A critical role for the autophagy gene Atg5 in T cell survival and proliferation. J Exp Med. 2007;204(1):25–31.
12. Miller BC, Zhao Z, Stephenson LM, Cadwell K, Pua HH, Lee HK, Mizushima NN, Iwasaki A, He YW, Swat W, Virgin HWT. The autophagy gene ATG5 plays an essential role in B lymphocyte development. Autophagy. 2008;4(3):309–14.
13. Baerga R, Zhang Y, Chen PH, Goldman S, Jin S. Targeted deletion of autophagy-related 5 (atg5) impairs adipogenesis in a cellular model and in mice. Autophagy. 2009;5(8):1118–30.
14. Singh R, Xiang Y, Wang Y, Baikati K, Cuervo AM, Luu YK, Tang Y, Pessin JE, Schwartz GJ, Czaja MJ. Autophagy regulates adipose mass and differentiation in mice. J Clin Invest. 2009;119(11):3329–39.
15. Zhang Y, Goldman S, Baerga R, Zhao Y, Komatsu M, Jin S. Adipose-specific deletion of autophagy-related gene 7 (atg7) in mice reveals a role in adipogenesis. Proc Natl Acad Sci USA. 2009;106(47):19860–5.
16. Levine B, Kroemer G. Autophagy in the pathogenesis of disease. Cell. 2008;132(1):27–42.
17. Hocking LJ, Whitehouse C, Helfrich MH. Autophagy: a new player in skeletal maintenance?. J Bone Miner Res. 2012;27(7):1439–47.
18. Manolagas SC, Parfitt AM. What old means to bone. Trends Endocrinol Metab. 2010;21(6):369–74.
19. Srinivas V, Bohensky J, Zahm AM, Shapiro IM. Autophagy in mineralizing tissues: microenvironmental perspectives. Cell Cycle. 2009;8(3):391–3.
20. Zhang L, Guo YF, Liu YZ, Liu YJ, Xiong DH, Liu XG, Wang L, Yang TL, Lei SF, Guo Y, Yan H, Pei YF, Zhang F, Papasian CJ, Recker RR, Deng HW. Pathway-based genome-wide association analysis identified the importance of regulation-of-autophagy pathway for ultradistal radius BMD. J Bone Miner Res. 2010;25(7):1572–80.
21. Pan F, Liu XG, Guo YF, Chen Y, Dong SS, Qiu C, Zhang ZX, Zhou Q, Yang TL, Guo Y, Zhu XZ, Deng HW. The regulation-of-autophagy pathway may influence Chinese stature variation: evidence from elder adults. J Hum Genet. 2010;55(7):441–7.
22. Zahm AM, Bohensky J, Adams CS, Shapiro IM, Srinivas V. Bone cell autophagy is regulated by environmental factors. Cells Tissues Organs. 2011;194(2–4):274–8.
23. Xia X, Kar R, Gluhak-Heinrich J, Yao W, Lane NE, Bonewald LF, Biswas SK, Lo WK, Jiang JX. Glucocorticoid-induced autophagy in osteocytes. J Bone Miner Res. 2010;25(11):2479–88.
24. Jia J, Yao W, Guan M, Dai W, Shahnazari M, Kar R, Bonewald L, Jiang JX, Lane NE. Glucocorticoid dose determines osteocyte cell fate. FASEB J. 2011;25(10):3366–76.
25. DeSelm CJ, Miller BC, Zou W, Beatty WL, van Meel E, Takahata Y, Klumperman J, Tooze SA, Teitelbaum SL, Virgin HW. Autophagy proteins regulate the secretory component of osteoclastic bone resorption. Dev Cell. 2011;21(5):966–74.
26. Whitehouse CA, Waters S, Marchbank K, Horner A, McGowan NW, Jovanovic JV, Xavier GM, Kashima TG, Cobourne MT, Richards GO, Sharpe PT, Skerry TM, Grigoriadis AE, Solomon E. Neighbor of Brca1 gene (Nbr1) functions as a negative regulator of postnatal osteoblastic bone formation and p38 MAPK activity. Proc Natl Acad Sci USA. 2010;107(29):12913–8.
27. Abbi S, Ueda H, Zheng C, Cooper LA, Zhao J, Christopher R, Guan JL. Regulation of focal adhesion kinase by a novel protein inhibitor FIP200. Mol Biol Cell. 2002;13(9):3178–91.
28. Ueda H, Abbi S, Zheng C, Guan JL. Suppression of Pyk2 kinase and cellular activities by FIP200. J Cell Biol. 2000;149(2):423–30.
29. Gan B, Guan JL. FIP200, a key signaling node to coordinately regulate various cellular processes. Cell Signal. 2008;20(5):787–94.
30. Hara T, Takamura A, Kishi C, Iemura S, Natsume T, Guan JL, Mizushima N. FIP200, a ULK-interacting protein, is required for autophagosome formation in mammalian cells. J Cell Biol. 2008;181(3):497–510.
31. Hosokawa N, Hara T, Kaizuka T, Kishi C, Takamura A, Miura Y, Iemura S, Natsume T, Takehana K, Yamada N, Guan JL, Oshiro N, Mizushima N. Nutrient-dependent mTORC1 association with the ULK1-Atg13-FIP200 complex required for autophagy. Mol Biol Cell. 2009;20(7):1981–91.
32. Jung CH, Jun CB, Ro SH, Kim YM, Otto NM, Cao J, Kundu M, Kim DH. ULK-Atg13-FIP200 complexes mediate mTOR signaling to the autophagy machinery. Mol Biol Cell. 2009;20(7):1992–2003.
33. Ganley IG, Lam du H, Wang J, Ding X, Chen S, Jiang X. ULK1.ATG13.FIP200 complex mediates mTOR signaling and is essential for autophagy. J Biol Chem. 2009;284(18):12297–305.
34. Liang CC, Wang C, Peng X, Gan B, Guan JL. Neural-specific deletion of FIP200 leads to cerebellar degeneration caused by increased neuronal death and axon degeneration. J Biol Chem. 2010;285(5):3499–509.
35. Liu F, Lee JY, Wei H, Tanabe O, Engel JD, Morrison SJ, Guan JL. FIP200 is required for the cell-autonomous maintenance of fetal hematopoietic stem cells. Blood. 2010;116(23):4806–14.
36. Hara T, Nakamura K, Matsui M, Yamamoto A, Nakahara Y, Suzuki-Migishima R, Yokoyama M, Mishima K, Saito I, Okano H, Mizushima N. Suppression of basal autophagy in neural cells causes neurodegenerative disease in mice. Nature. 2006;441(7095):885–9.
37. Komatsu M, Waguri S, Chiba T, Murata S, Iwata J, Tanida I, Ueno T, Koike M, Uchiyama Y, Kominami E, Tanaka K. Loss of autophagy in the central nervous system causes neurodegeneration in mice. Nature. 2006;441(7095):880–4.
38. Komatsu M, Waguri S, Koike M, Sou YS, Ueno T, Hara T, Mizushima N, Iwata J, Ezaki J, Murata S, Hamazaki J, Nishito Y, Iemura S, Natsume T, Yanagawa T, Uwayama J, Warabi E, Yoshida H, Ishii T, Kobayashi A, Yamamoto M, Yue Z, Uchiyama Y, Kominami E, Tanaka K. Homeostatic levels of p62 control cytoplasmic inclusion body formation in autophagy-deficient mice. Cell. 2007;131(6):1149–63.
39. Mortensen M, Soilleux EJ, Djordjevic G, Tripp R, Lutteropp M, Sadighi-Akha E, Stranks AJ, Glanville J, Knight S, Jacobsen SE, Kranc KR, Simon AK. The autophagy protein Atg7 is essential for hematopoietic stem cell maintenance. J Exp Med. 2011;208(3):455–67.
40. Wei H, Wei S, Gan B, Peng X, Zou W, Guan JL. Suppression of autophagy by FIP200 deletion inhibits mammary tumorigenesis. Genes Dev. 2011;25(14):1510–27.
41. Bae H, Guan JL. Suppression of autophagy by FIP200 deletion impairs DNA damage repair and increases cell death upon treatments with anticancer agents. Mol Cancer Res. 2011;9(9):1232–41.
42. Wang C, Liang CC, Bian ZC, Zhu Y, Guan JL. FIP200 is required for maintenance and differentiation of postnatal neural stem cells. Nat Neurosci. 2013;16(5):532–42.
43. Gan B, Peng X, Nagy T, Alcaraz A, Gu H, Guan JL. Role of FIP200 in cardiac and liver development and its regulation of TNFalpha and TSC-mTOR signaling pathways. J Cell Biol. 2006;175(1):121–33.

44. Rodda SJ, McMahon AP. Distinct roles for Hedgehog and canonical Wnt signaling in specification, differentiation and maintenance of osteoblast progenitors. Development. 2006;133(16):3231–44.
45. Liu F, Woitge HW, Braut A, Kronenberg MS, Lichtler AC, Mina M, Kream BE. Expression and activity of osteoblast-targeted Cre recombinase transgenes in murine skeletal tissues. Int J Dev Biol. 2004;48(7):645–53.
46. Mizushima N, Yamamoto A, Matsui M, Yoshimori T, Ohsumi Y. In vivo analysis of autophagy in response to nutrient starvation using transgenic mice expressing a fluorescent autophagosome marker. Mol Biol Cell. 2004;15(3):1101–11.
47. McLeod MJ. Differential staining of cartilage and bone in whole mouse fetuses by alcian blue and alizarin red S. Teratology. 1980;22 (3):299–301.
48. Feldkamp LA, Goldstein SA, Parfitt AM, Jesion G, Kleerekoper M. The direct examination of three-dimensional bone architecture in vitro by computed tomography. J Bone Miner Res. 1989;4(1):3–11.
49. McCreadie BR, Goulet RW, Feldkamp LA, Goldstein SA. Hierarchical structure of bone and micro-computed tomography. Adv Exp Med Biol. 2001;496:67–83.
50. Kuhn JL, Goldstein SA, Feldkamp LA, Goulet RW, Jesion G. Evaluation of a microcomputed tomography system to study trabecular bone structure. J Orthop Res. 1990;8(6):833–42.
51. Meganck JA, Kozloff KM, Thornton MM, Broski SM, Goldstein SA. Beam hardening artifacts in micro-computed tomography scanning can be reduced by X-ray beam filtration and the resulting images can be used to accurately measure BMD. Bone. 2009;45(6):1104–16.
52. Volkman SK, Galecki AT, Burke DT, Miller RA, Goldstein SA. Quantitative trait loci that modulate femoral mechanical properties in a genetically heterogeneous mouse population. J Bone Miner Res. 2004;19(9):1497–505.
53. Volkman SK, Galecki AT, Burke DT, Paczas MR, Moalli MR, Miller RA, Goldstein SA. Quantitative trait loci for femoral size and shape in a genetically heterogeneous mouse population. J Bone Miner Res. 2003;18(8):1497–505.
54. Liu F, Lee SK, Adams DJ, Gronowicz GA, Kream BE. CREM deficiency in mice alters the response of bone to intermittent parathyroid hormone treatment. Bone. 2007;40(4):1135–43.
55. Chandhoke TK, Huang YF, Liu F, Gronowicz GA, Adams DJ, Harrison JR, Kream BE. Osteopenia in transgenic mice with osteoblast-targeted expression of the inducible cAMP early repressor. Bone. 2008;43(1):101–9.
56. Parfitt AM, Drezner MK, Glorieux FH, Kanis JA, Malluche H, Meunier PJ, Ott SM, Recker RR. Bone histomorphometry: standardization of nomenclature, symbols, and units. Report of the ASBMR Histomorphometry Nomenclature Committee. J Bone Miner Res. 1987;2 (6):595–610.
57. Mizushima N, Yoshimori T, Levine B. Methods in mammalian autophagy research. Cell. 2010;140(3):313–26.
58. Slack-Davis JK, Martin KH, Tilghman RW, Iwanicki M, Ung EJ, Autry C, Luzzio MJ, Cooper B, Kath JC, Roberts WG, Parsons JT. Cellular characterization of a novel focal adhesion kinase inhibitor. J Biol Chem. 2007;282(20):14845–52.
59. Stokes JB, Adair SJ, Slack-Davis JK, Walters DM, Tilghman RW, Hershey ED, Lowrey B, Thomas KS, Bouton AH, Hwang RF, Stelow EB, Parsons JT, Bauer TW. Inhibition of focal adhesion kinase by PF-562,271 inhibits the growth and metastasis of pancreatic cancer concomitant with altering the tumor microenvironment. Mol Cancer Ther. 2011;10(11):2135–45.
60. Gomes LC, Di Benedetto G, Scorrano L. During autophagy mitochondria elongate, are spared from degradation and sustain cell viability. Nat Cell Biol. 2011;13(5):589–98.
61. Rabinowitz JD, White E. Autophagy and metabolism. Science. 2010;330(6009):1344–8.
62. Yang Z, Klionsky DJ. Eaten alive: a history of macroautophagy. Nat Cell Biol. 2010;12(9):814–22.
63. Fimia GM, Stoykova A, Romagnoli A, Giunta L, Di Bartolomeo S, Nardacci R, Corazzari M, Fuoco C, Ucar A, Schwartz P, Gruss P, Piacentini M, Chowdhury K, Cecconi F. Ambra1 regulates autophagy and development of the nervous system. Nature. 2007;447 (7148):1121–5.
64. Komatsu M, Waguri S, Ueno T, Iwata J, Murata S, Tanida I, Ezaki J, Mizushima N, Ohsumi Y, Uchiyama Y, Kominami E, Tanaka K, Chiba T. Impairment of starvation-induced and constitutive autophagy in Atg7-deficient mice. J Cell Biol. 2005;169(3):425–34.
65. Yue Z, Jin S, Yang C, Levine AJ, Heintz N. Beclin 1, an autophagy gene essential for early embryonic development, is a haploinsufficient tumor suppressor. Proc Natl Acad Sci USA. 2003;100 (25):15077–82.
66. Mijaljica D, Prescott M, Devenish RJ. Different fates of mitochondria: alternative ways for degradation?. Autophagy. 2007;3(1):4–9.
67. Hara T, Mizushima N. Role of ULK-FIP200 complex in mammalian autophagy: FIP200, a counterpart of yeast Atg17?. Autophagy. 2009;5(1):85–7.
68. Kim JB, Leucht P, Luppen CA, Park YJ, Beggs HE, Damsky CH, Helms JA. Reconciling the roles of FAK in osteoblast differentiation, osteoclast remodeling, and bone regeneration. Bone. 2007;41 (1):39–51.
69. Buckbinder L, Crawford DT, Qi H, Ke HZ, Olson LM, Long KR, Bonnette PC, Baumann AP, Hambor JE, Grasser WA 3rd, Pan LC, Owen TA, Luzzio MJ, Hulford CA, Gebhard DF, Paralkar VM, Simmons HA, Kath JC, Roberts WG, Smock SL, Guzman-Perez A, Brown TA, Li M. Proline-rich tyrosine kinase 2 regulates osteoprogenitor cells and bone formation, and offers an anabolic treatment approach for osteoporosis. Proc Natl Acad Sci USA. 2007;104 (25):10619–24.
70. Wullschleger S, Loewith R, Hall MN. TOR signaling in growth and metabolism. Cell. 2006;124(3):471–84.
71. Mizushima N. The role of the Atg1/ULK1 complex in autophagy regulation. Curr Opin Cell Biol. 2010;22(2):132–9.
72. Narita M, Young AR, Arakawa S, Samarajiwa SA, Nakashima T, Yoshida S, Hong S, Berry LS, Reichelt S, Ferreira M, Tavare S, Inoki K, Shimizu S. Spatial coupling of mTOR and autophagy augments secretory phenotypes. Science. 2011;332(6032):966–70.
73. Hubbard VM, Valdor R, Macian F, Cuervo AM. Selective autophagy in the maintenance of cellular homeostasis in aging organisms. Biogerontology. 2012;13(1):21–35.
74. Spilman P, Podlutskaya N, Hart MJ, Debnath J, Gorostiza O, Bredesen D, Richardson A, Strong R, Galvan V. Inhibition of mTOR by rapamycin abolishes cognitive deficits and reduces amyloid-beta levels in a mouse model of Alzheimer's disease. PLoS One. 2010;5 (4):e9979.
75. Shoji-Kawata S, Sumpter R, Leveno M, Campbell GR, Zou Z, Kinch L, Wilkins AD, Sun Q, Pallauf K, MacDuff D, Huerta C, Virgin HW, Helms JB, Eerland R, Tooze SA, Xavier R, Lenschow DJ, Yamamoto A, King D, Lichtarge O, Grishin NV, Spector SA, Kaloyanova DV, Levine B. Identification of a candidate therapeutic autophagy-inducing peptide. Nature. 2013;494(7436):201–6.